Far-Reaching Effects of the Hawaiian Islands on the Pacific Ocean–Atmosphere System

Shang-Ping Xie,[1]* W. Timothy Liu,[2] Qinyu Liu,[3] Masami Nonaka[1]†

Using satellite data, we detected a wind wake trailing westward behind the Hawaiian Islands for 3000 kilometers, a length many times greater than observed anywhere else on Earth. This wind wake drives an eastward ocean current that draws warm water from the Asian coast 8000 kilometers away, leaving marked changes in surface and subsurface ocean temperature. Standing in the path of the steady trade winds, Hawaii triggers an air-sea interaction that provides the feedback to sustain the influence of these small islands over a long stretch of the Pacific Ocean.

In a strongly stratified atmosphere, an isolated ocean island of high elevation forces the impinging air flow to split, generating a wake of weak winds downstream and stronger-than-ambient winds on the flanks. Because the height of waves generated by local wind instead of swells increases with wind speed, the ocean surface tends to be smooth under the weak wind conditions in the wake and rough under the strong wind conditions outside the wake. Such contrast in surface roughness behind an island is often visible from aerial views and in satellite sunglint (*1*) and scatterometer (*2*) images. Under certain conditions, wind wakes can become unstable, leading to the formation of spectacular vortex streets (*3*–*5*). Standing in the steady northeast trade winds and far away from a major landmass, the Hawaiian Islands are an ideal natural laboratory for studying wake phenomena.

In summer, Hawaii is under the control of a strong Pacific-wide subtropical high. The well-mixed planetary boundary layer (PBL) is capped by a strong temperature inversion at around 1 to 2 km height. The elevation of the major Hawaiian Islands generally exceeds 1 km. Particularly, Haleakala (3055 m) on Maui and Mauna Loa (4169 m) and Mauna Kea (4201 m) on the island of Hawaii (hereafter the Big Island) penetrate far above the trade inversion. The high-resolution QuikSCAT satellite (*6*) reveals that a wake of weak winds forms behind each of the major Hawaiian Islands (Fig. 1): Kauai, Oahu, Molokai-Lanai-Maui, and the Big Island (*7*). The weak winds in the wake and the strong winds on the flanks generate four pairs of dipole vorticity anomalies, with positive vorticity to the north and negative vorticity to the south. (The vorticity signal of the Kauai wake is weak.) These individual wakes of the separate Hawaiian Islands start to dissipate and become much less distinct about 300 km downstream as a result of surface drag and mixing [appendix A in (*8*)]. Even further downstream, a wide band of weaker winds appears.

A broad satellite view of the subtropical North Pacific reveals that the influence of Hawaii extends far west (Fig. 2). The wind speed minimum can be seen to 175°W, beyond which it is obscured by the strong background gradient. The curl and convergence (or cloud water) of wind velocity, whose spatial derivative helps filter out the large-scale background fields, trace the island-induced wind anomalies as far west as 175°E, just north of the Marshall Islands [Fig. 2 and appendix B in (*8*)]. This 3000-km wake is 10 times longer than any individual island wake observed until now. Such a long-lasting influence of Hawaii is not unique to the year 1999 and stands out in the climatology of the central North Pacific. Our analysis of longer term satellite observations confirms that the island influences extend to 175°E [appendix B in (*8*)].

In order to investigate the physical mechanisms that sustain this Hawaiian wake over such a great distance against dissipation, we use additional observations of sea surface temperature (SST), wind speed, and cloud liquid water (LW) from the Tropical Rain Measuring Mission (TRMM) satellite (*9*). We will show that the ocean, by adjusting its SST, provides the feedback necessary for the wake's great extension to the west.

SST generally decreases poleward. West of Hawaii, however, SST reverses its meridional gradient around 15°N, reaching a local maximum around 19°N. This creates a peculiar warm tongue that extends far from the western Pacific and stops abruptly at Hawaii. To the south is a cold tongue that emanates from the southern tip of the Big Island and extends westward. The TRMM satellite detects a definite atmospheric response to this change in the meridional SST gradient: A band of high cloud LW forms directly over the warm tongue, whereas relatively clear skies prevail over the cold tongue to the south (Fig. 2C). This high-LW band is most likely associated with low-level clouds, given the strong capping of the PBL in this subtropical region. The surface wind speed distribution (Fig. 2B) provides further evidence of an atmospheric response to the warm tongue. The local wind speed minimum is located between the warm and cold tongues and is flanked by two higher wind zones. The wind speed difference between the wake and high-wind zones is typically 0.5 m/s. The northern high-wind zone apparently originates from Kauai and is then reinvigorated around 165°W, probably in response to the warm tongue.

The background trade winds have a much broader meridional scale than the Hawaiian Island chain and its wake. In order to highlight the narrow wake, we apply an 8° moving average in the meridional direction and remove it as the background state. Whereas east of 155°W this high-pass filtered map is nearly featureless, west of the Islands a band of high SSTs appears that stretches along 19°N to 175°W and then slants gently toward the southwest. Anomalous meridional winds converge onto this warm water band (Fig. 3), supplying the moisture for the cloud band seen in Fig. 2C. This association between meridional wind and SST gradient on the flanks of the warm tongue can be traced to west of the international dateline. The fact that separate measurements by independent satellites come together and fit into a physically consistent picture gives us confidence in our results.

What causes the warm water band? We first consider surface processes such as heat flux and upwelling that are major mechanisms for SST changes in the equatorial oceans (*10*–*12*). The filtered map shows that the anomalous wind vectors just behind the Hawaiian Islands are roughly symmetric about the centerline of the warm water band. West of 165°W, the Coriolis force acts on the converging meridional winds, and the zonal winds become asymmetric—westerly on the southern edge and easterly on the northern edge of the warm band. South of the warm band's center, these anomalous winds weaken the background northeasterly trades, reducing evaporative cooling at the ocean surface and increasing SSTs; north of the band's center, the winds enhance the trades, increasing evaporation and lowering SSTs. In the tropics, interaction among wind, evaporation,

[1]International Pacific Research Center, School of Ocean and Earth Science and Technology, University of Hawaii, 2525 Correa Road, Honolulu, HI 96822, USA. [2]Jet Propulsion Laboratory, California Institute of Technology, 4800 Oak Grove Drive, Pasadena, CA 91109, USA. [3]Physical Oceanography Laboratory, Ocean University of Qingdao, Qingdao 266003, China.

*To whom correspondence should be addressed. E-mail: xie@soest.hawaii.edu

†Also at Frontier Research System for Global Change, Yokohama 236–0001, Japan.

and SST provides a positive feedback and shapes the spatial (*10*) and temporal (*11*) variability of the climate. In the subtropics, however, the interaction becomes stable and cannot sustain the higher SSTs in the warm band, because the strong Coriolis effect forces a 90° meridional phase difference between anomalous SST and wind speed. (Instead, this interaction creates a tendency for SST anomalies to move southward.) Moreover, the locally enhanced cloud LW over the warm band reflects more sunlight into space and acts to lower SSTs. The local Ekman pumping velocity is anomalously upward over the high SST band and again is a damper, if anything (*12*).

With the surface processes eliminated as the cause of the warm band, we now turn to the subsurface ocean. The Hawaiian Islands block a broad westward-flowing North Equatorial Current (NEC). West of the islands, an eastward current, the Hawaiian Lee Counter Current (HLCC), is observed along 19°N (*13*). In boreal summer when a strong zonal SST gradient is observed between 15° and 25°N, the warm advection by this HLCC amounts to a substantial heat flux of 30 Wm^{-2} for a 50-m-deep mixed layer. We thus suggest that HLCC's warm advection causes the warm tongue west of Hawaii.

The HLCC has only recently been identified from a painstaking analysis of historical data (*14*). Our analysis below indicates that the dipole wind curl in the Hawaiian wake is a major driving force. In general, wind curl drives geostrophic currents by vertically displacing the thermocline both locally and via westward-traveling Rossby waves. The resultant ocean circulation has the same rotation as the wind curl. Consistent with the Ekman pumping pattern in Fig. 2A, the observed HLCC straddles an anticyclonic and a cyclonic circulation to the south and north, respectively [fig. 5 of (*13*)].

We used three ocean models with different physics to infer what causes the HLCC. The first is a high-resolution (1/4° × 1/4°) ocean general circulation model (GCM) forced by the wind product of the European Center for Medium-range Weather Forecast analysis that assimilates satellite scatterometer data (*15*, *16*). The model reproduces the HLCC at the observed latitude and speed (Fig. 4A). The second is also an ocean GCM, but its 1° × 1° resolution does not permit mesoscale eddies (*17*). The HLCC is reproduced west of Hawaii but is only half as strong. The third is a linear reduced-gravity model, which again reproduces the HLCC [appendix C of (*8*) compares these models in more detail]. The success of the third model, which contains only the Sverdrup dynamics, supports the wind-driven mechanism for the HLCC, a conclusion corroborated by the observed thermocline structure. In contrast to its gradual northward deepening east of Hawaii, the thermocline displays a peculiar shoaling between 18° and 20°N west of the islands, which is indicative of an eastward geostrophic current near the surface (Fig. 4, C and D).

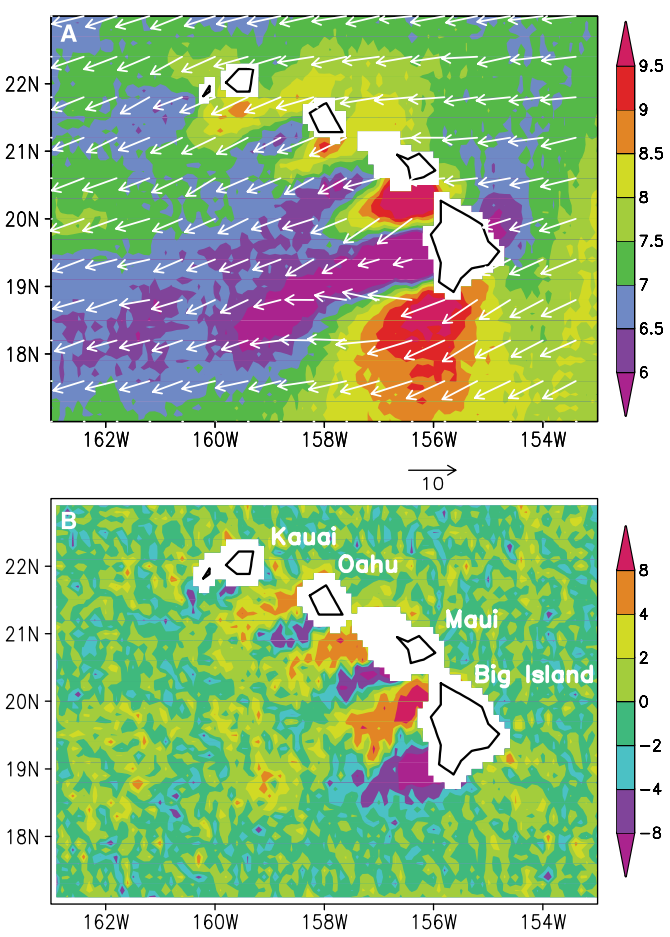

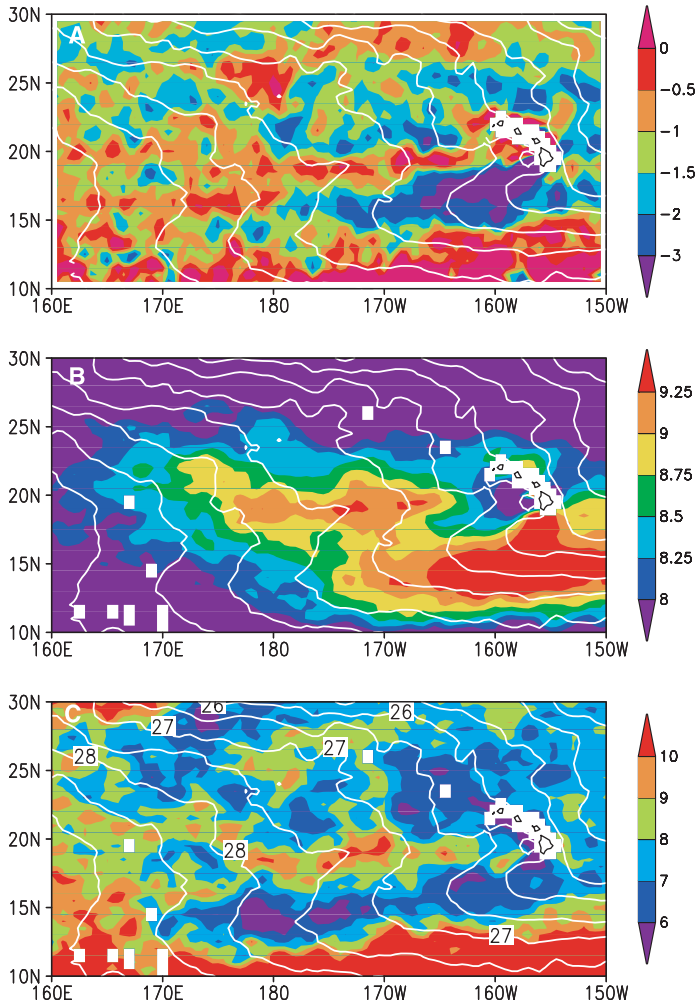

Fig. 1 (left). (**A**) Wind speed (color scale is in m s^{-1}) and velocity vectors, and (**B**) wind curl (10^{-5} s^{-1}) observed by the QuikSCAT satellite for 1 to 31 August 1999. **Fig. 2 (right).** (**A**) Ekman pumping velocity (10^{-6} m s^{-1}); (**B**) wind speed (m s^{-1}); and (**C**) cloud LW (10^{-2} mm) and SST (white contours at 0.5°C intervals), averaged for 21 July to 31 October 1999. Ekman pumping velocity (We) is defined as We = curl(τ/f)/ρ, where τ is the wind stress vector, f is the Coriolis parameter, and ρ is the water density. Because f changes only gradually with latitude, most features in (A) result from the wind curl.

Figure 4A suggests that the eastward current is not confined to the vicinity of Hawaii but extends all the way into the western Pacific and covers a distance of 8000 km. This narrow current, which starts in the western Pacific and ends abruptly at Hawaii, can often be seen in operational surface current analyses in Japan Meteorological Agency (JMA) Monthly Marine Reports. The western portion of this eastward current has long been known to Japanese scientists and is called the subtropical countercurrent (*18*). Its cause, however, remains poorly understood. Although thermal forcing plays a role (*19*, *20*), the continuous westward extension of the countercurrent shown in Fig. 4A is indicative of Rossby wave adjustment in response to the Hawaii-induced wind curl (*21*, *22*). Imbedded in the broad westward NEC and in a background SST field increasing toward the west, this eastward countercurrent leaves a distinct signature as a warm current even in the annual mean SST climatology (Fig. 4A).

Thus, the long Hawaiian wake should be viewed as the coupled ocean-atmosphere response to perturbation by the islands. The chain of interaction may be summarized as follows. As the broad, steady northeasterly trades impinge on Hawaii, a number of mechanical wakes form behind the individual islands. These individual wakes dissipate rather quickly, and a broad wake takes their place 300 km downwind. The wind curl associated with this broader wake forces oceanic Rossby waves and generates an eastward current that advects warmer water from the west, giving rise to a warm SST tongue pointing toward Hawaii. The attendant SST gradient forces meridional winds to converge, and a local maximum in cloud LW forms. These anomalous winds weaken the northeasterly trades south of the warm tongue and intensify the northeasterly trades north of the warm tongue, allowing the wake and the wind curl pattern to persist over a great distance.

Wakes behind ocean islands are commonly observed, but they usually do not affect large-scale ocean circulation because of synoptic/seasonal changes in wind direction. Owing to the steady trades and the broad width of the island chain, the Hawaiian wake exerts a steady and substantial forcing on the ocean. This gives rise to the unique attributes of the Hawaiian wake: its long tail and its interaction with the ocean. How the atmosphere responds to extratropical SST anomalies is poorly understood and is a stumbling

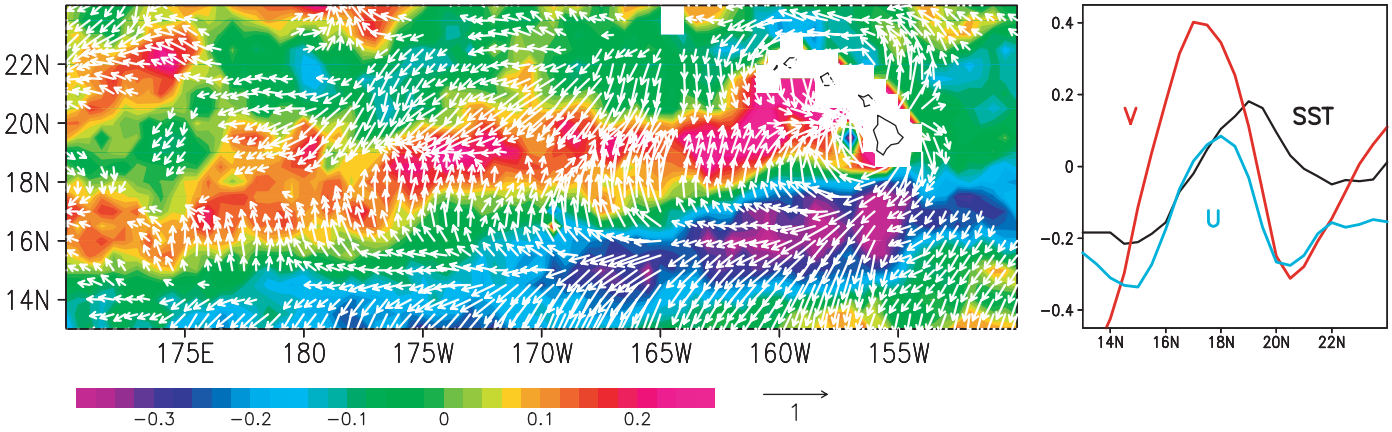

Fig. 3. (**Left**) High-pass filtered SST (color scale is in °C) and wind vectors (m s^{-1}), along with (**right**) their zonal averages for 175°W to 165°W. The vector scale is changed to 3 m s^{-1} for winds east of 165°W for clarity. The latitudinal filtering is done by subtracting an 8° moving average from the original data to remove the large-scale background fields. *U* and *V* are zonal and meridional wind velocities, respectively.

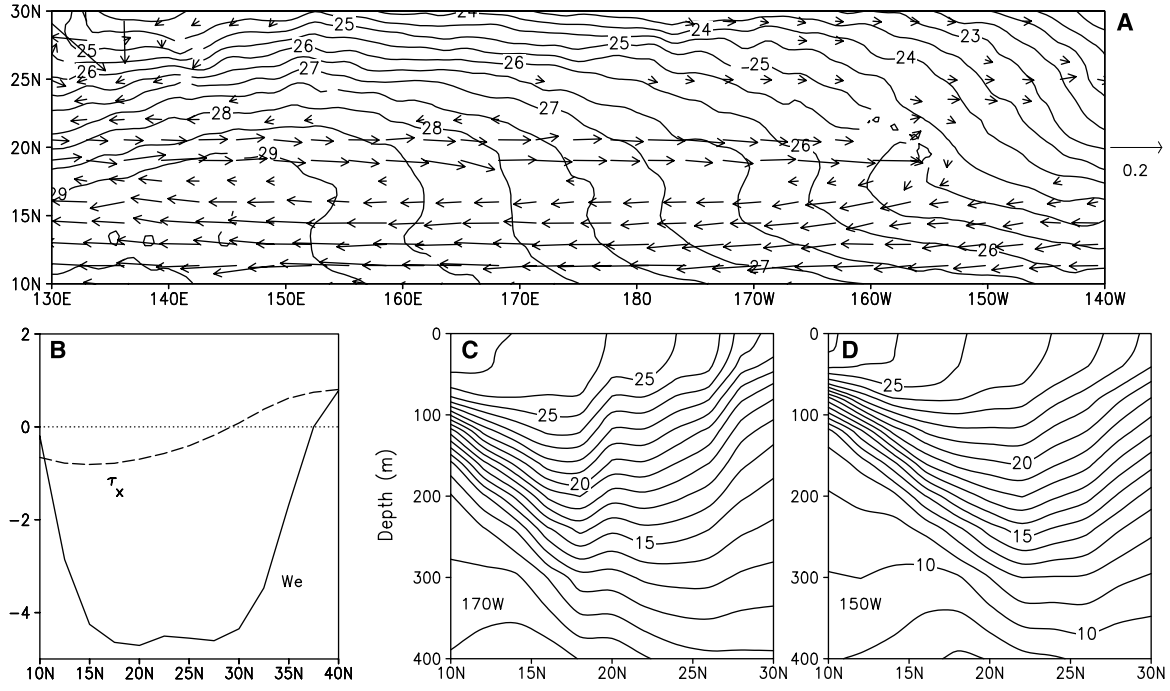

Fig. 4. (**A**) Current vectors (in m s^{-1}) at 37.5 m averaged for 1992–98 in a high-resolution ocean GCM and annual mean SST (contours in °C) for 1999 observed by the TRMM satellite. (**B**) Climatological mean zonal wind stress [τ_x, in N m^{-2} (*29*)] and Ekman pumping velocity (10^{-6} m s^{-1}) averaged for 155°E to 170°W as a function of latitude. Observed ocean temperature (*30*) (in °C) averaged for 1959–98 as a function of latitude and depth is shown (**C**) west and (**D**) east of Hawaii.

block to further progress in the study of non–El Niño climate variability (*23*, *24*). Our results demonstrate that surface winds react to modest subtropical SST variations as small as a few tenths of a degree. The simulation of the far-reaching effects of Hawaii can serve as a test for the next generation of high-resolution climate models.

The physical processes we have described here probably give rise to other changes in the Pacific Ocean and atmosphere. For instance, Hawaii, with its volcanic and human activities, is a major aerosol source for the surrounding region. The long convergence line in the wind wake detected in this study may influence the transport of aerosols and trace gases in the PBL and their exchange with the free atmosphere. Regarding the ocean, the banded structures in upwelling velocity may lead to variations in the distributions of plankton and other fishery resources.

References and Notes

1. R. B. Smith, A. C. Gleason, P. A. Gluhosky, V. Grubisic, *J. Atmos. Sci*. **54**, 606 (1997).
2. M. H. Freilich, Orographically Modified Winds Observed by the NASA Scatterometer (1997) (available at www.oce.orst.edu/po/research/mhf/).
3. K. P. Chopra, *Adv. Geophys.* **16**, 298 (1973).
4. D. Etling, *Meteorol. Atmos. Phys*. **41**, 157 (1989).
5. T. P. DeFelice, D. J. Meyer, G. Xian, J. Christopherson, R. Cahalan, *Bull. Am. Meteorol. Soc*. **81**, 1047 (2000).
6. W. T. Liu, X. Xie, P. S. Polito, S.-P. Xie, H. Hashizume, *Geophys. Res. Lett*. **27**, 2545 (2000).
7. The winds on and near the Big Island have been the focus of previous field campaigns (*25*, *26*). Reduced wind speed on the windward side of the Big Island results from orographic blocking (Fig. 1). The strongest winds are found between Maui and the Big Island, reaching 11 m/s in the monthly-mean map of Fig. 1 in comparison to the ambient speed of 7 m/s. The winds between these two tallest islands can often exceed 20 m/s, and these strong winds are blamed for having damaged the foremast of the ship *Resolution* in 1779, forcing Captain James Cook to make his fatal return trip to the Big Island. The strong positive wind curl probably contributes to the formation of the cold eddies often observed northwest of the Big Island (*27*).
8. Supplementary Web material is available on *Science* Online at www.sciencemag.org/cgi/content/full/292/5524/2057/DC1.
9. F. J. Wentz, C. Gentemann, D. Smith, D. Chelton, *Science* **288**, 847 (2000).
10. S.-P. Xie, S. G. H. Philander, *Tellus* **46A**, 340 (1994).
11. P. Chang, L. Ji, H. Li, *Nature* **385**, 516 (1997).
12. T. Yamagata, in *Coupled Ocean-Atmosphere Model*, J. C. J. Nihoul, Ed. (Elsevier, New York, 1985), pp. 637–657.
13. B. Qiu, D. A. Koh, C. Lumpkin, P. Flament, *J. Phys. Oceanogr*. **27**, 431 (1997).
14. P. Flament, S. Kennan, R. Lumpkin, M. Sawyer, E. Stroup, in *Atlas of Hawaii*, S. P. Juvik, J. O. Juvik, Eds. (Univ. of Hawaii Press, Honolulu, HI, 1998), pp. 82–86.
15. D. Stammer, R. Tokmakian, A. J. Semtner, C. Wunsch, *J. Geophys. Res*. **101**, 25779 (1996).
16. Q. Liu, H. Yang, H. Bao, W. Li, *Chin. J. Atmos. Sci*. **24**, 363 (2000).
17. S.-P. Xie, T. Kunitani, A. Kubokawa, M. Nonaka, S. Hosoda, *J. Phys. Oceanogr*. **30**, 2798 (2000).
18. K. Yoshida, T. Kidokoro, *J. Oceanogr. Soc. Jpn*. **23**, 88 (1967).
19. K. Takeuchi, *J. Phys. Oceanogr*. **16**, 919 (1986).
20. A. Kubokawa, T. Inui, *J. Phys. Oceanogr*. **29**, 1303 (1999).
21. West of Hawaii, ocean current direction is especially sensitive to the curl of the wind wake off the islands, because the large-scale Ekman pumping field has little meridional gradient (Fig. 4B) to drive background zonal current.
22. The existing in situ measurements are insufficient to ascertain the western extent of the eastward countercurrent that ends at Hawaii, but a hydrographic section maintained by the Japan Meterological Agency along 137°E since 1967 hints at its existence in the far western Pacific. Geostrophic calculation using the long-term mean data in this 137°E section indicates that at 19°N, the eastward shear reaches a meridional maximum in the upper 300 m, and the current, albeit weak, is eastward near the surface (*28*). The use of new satellite data here allows us to determine for the first time that the high mountains on the Hawaiian Islands, by blocking the air flow, are the ultimate cause of this eastward countercurrent along 19°N [appendix C in (*8*)].
23. Y. Okumura, S.-P. Xie, A. Numaguti, Y. Tanimoto, *Geophys. Res. Lett*. **28**, 1507 (2001).
24. W. A. Robinson, *Bull. Am. Meteorol. Soc*. **77**, 567 (2000).
25. R. B. Smith, V. Grubisic, *J. Atmos. Sci*. **50**, 3728 (1993).
26. E. C. Nickerson, M. A. Dias, *J. Appl. Meteorol*. **20**, 868 (1981).
27. W. C. Patzert, *Hawaii Inst. Geophys. Rep*. *69-8* (1969).
28. W. B. White, A. E. Walker, *J. Geophys. Res*. **90**, 7061 (1985)
29. E. Kalnay *et al*., *Bull. Am. Meteorol. Soc*. **77**, 437 (1996).
30. W. B. White, *Progr. Oceanogr*. **36**, 169 (1995).

31. We thank B. Qiu and G. Speidel for comments and W. Tang, X. Xie, A. Pan, P. Broccio, R. Tokmakian, H. Okajima, Y. Okumura and J. Hafner for data processing and graphics. The Special Sensor Microwave/Imager and TRMM data were produced by F. Wentz at Remote Sensing Systems, who generously made them openly accessible. The European Remote-Sensing Satellite data were obtained via FTP from the Institut Français de Recherche pour l'Exploitation de la Mer. This study is supported by NASA under QuikSCAT and TRMM missions and grant NAG5-10045, by the Frontier Research System for Global Change, and by the National Natural Science Foundation of China (grant 49976004). W.T.L.'s work was performed at the Jet Propulsion Laboratory, California Institute of Technology, under contract with NASA. This is International Pacific Research Center contribution 92 and School of Ocean and Earth Science and Technology contribution 5579.

12 February 2001; accepted 7 May 2001

Linearly Polarized Emission from Colloidal Semiconductor Quantum Rods

Jiangtao Hu,[1,2]* Liang-shi Li,[1,2]* Weidong Yang,[1,2] Liberato Manna,[1,2] Lin-wang Wang,[3] A. Paul Alivisatos[1,2]†

Colloidal quantum rods of cadmium selenide (CdSe) exhibit linearly polarized emission. Empirical pseudopotential calculations predict that slightly elongated CdSe nanocrystals have polarized emission along the long axis, unlike spherical dots, which emit plane-polarized light. Single-molecule luminescence spectroscopy measurements on CdSe quantum rods with an aspect ratio between 1 and 30 confirm a sharp transition from nonpolarized to purely linearly polarized emission at an aspect ratio of 2. Linearly polarized luminescent chromophores are highly desirable in a variety of applications.

Colloidal semiconductor nanocrystals, or quantum dots, are a class of luminescent chromophores, which has emerged from the growing fields of nanoscience and nanotechnology (*1, 2*). The optical emission properties of these chromophores can be tailored by suitably adjusting the height, width, and shape of the potential that confines electrons and holes. In spherically shaped colloidal dots, the band gap and oscillator strength can be tuned by variation of the diameter (*3*). Colloidal dots can be produced by comparatively simple solution methods and are photochemically robust (*4, 5*). Compared to self-assembled quantum dots made by molecular beam epitaxy (*6, 7*), they have more chemical flexibility and have nearly the same optical and electrical performance (*8, 9*). Thus, colloidal quantum dots may have a very wide range of applications, e.g., as light emitters in biological labeling (*10, 11*), displays (*12, 13*), and lasers (*14*).

A limiting feature of the spherical colloidal dots is that their emission is not linearly polarized (*15, 16*). It has been suggested that colloidal rods may display polarized emission with significant advantages over spherical dots (*17*). Here, we combine recent advances in synthetic control of nanocrystal shapes, single-molecule spectroscopy, and electronic structure theory to study quantum rods. We studied CdSe nanocrystals because their synthesis has been well developed (*18*, *19*), so much so that they have become a model system for studying quantum size effects. Theory predicts a level crossing as a function of aspect ratio in colloidal quantum rods, such that slightly elongated dots (an aspect ratio of 2:1) should emit linearly polarized light. This prediction is qualitatively verified by

[1]Department of Chemistry, University of California at Berkeley, Berkeley, CA 94720, USA. [2]Materials Science Division, [3]National Energy Research Scientific Computing Center, Lawrence Berkeley National Laboratory, 1 Cyclotron Road, Berkeley, CA 94720, USA.

*These authors contributed equally to this work.
†To whom correspondence should be addressed.